

Dynamic mechanical behaviour and longitudinal crystal thickness measurements on ultra-high modulus linear polyethylene: a quantitative model for the elastic modulus

A. G. Gibson, G. R. Davies and I. M. Ward

Department of Physics, University of Leeds, Leeds LS2 9JT, UK

(Received 12 December 1977; revised 1 February 1978)

In this paper the dynamic mechanical behaviour of ultra-high modulus polyethylene is reported. The results are discussed in terms of a fibre reinforced composite model, in which the amount of fibre phase is related to the number of intercrystalline bridges determined from X-ray diffraction data. For both drawn and extruded materials a good correlation has been obtained between the plateau modulus at -50°C and the longitudinal crystal thickness. This correlation is given a quantitative interpretation in terms of the model and the increase in modulus with increasing deformation ratio is ascribed to an increase in continuity of the crystalline phase. The increase in tensile modulus on cooling through the γ -process is related primarily to the change in the tensile modulus of the amorphous phase. The fall in modulus at high temperature, on the other hand, indicates a fall in the shear modulus of the crystalline phase, which provides a satisfactory explanation of the α -process.

INTRODUCTION

This paper forms part of a series of publications dealing with the preparation and properties of ultra-high modulus polyolefines. As discussed in previous papers, two processes have been used, drawing^{1,2} and hydrostatic extrusion³. Although these processes differ in many respects they are both essentially solid phase tensile deformation processes, drawing being used to produce fibres and films, and hydrostatic extrusion solid shapes of substantial cross-section. In each case ultra-high modulus material of similar structure and properties can be produced and it has been noted that the overall deformation ratio is the main factor in determining the mechanical stiffness^{1,2}.

The main purpose of the present paper is to discuss the relationship between the mechanical behaviour and morphology in ultra-high modulus linear polyethylene (LPE) combining mechanical and structural data from both drawn and extruded materials. We will confine ourselves to the behaviour of one grade of LPE, Rigidex 50, although we believe that our conclusions will be relevant to other grades of LPE, and possibly to other ultra-high modulus oriented polymers such as polypropylene and polyoxymethylene.

The dynamic mechanical behaviour of samples from a range of draw ratios has been determined over a wide range of temperatures. As in a previous publication⁴ we will seek to relate the mechanical stiffness in a non-viscoelastic régime to the structure of the materials. In the present paper, we will draw upon small-angle and wide-angle X-ray measurements reported in the related publication⁵ to provide the required structural information, and show that the average crystalline sequence length as measured by the latter technique correlates directly with mechanical stiffness. A quantitative treatment is given for the mechanical modulus in terms of the proportion of intercrystalline bridges, this being estimated from the X-ray diffraction data. Our theoretical

model is analogous to a reinforced fibre composite model but the apparent 'fibre' content of the model is determined at each stage of the deformation by the number of intercrystalline bridges in the sample.

EXPERIMENTAL

Preparation of samples

Results will be presented for Rigidex 50, a linear ethylene homopolymer manufactured by BP Chemicals International Ltd. The weight- and number-average molecular weights were 101 450 and 6180, respectively and the melt flow index was 6.

Ultra-oriented samples of this material were prepared both by drawing and hydrostatic extrusion. The preparation details were as follows.

Drawing. Isotropic sheets for drawing were prepared by compression moulding granules at 170°C and then quenching into water at room temperature. Dumb-bell samples with gauge dimensions 2×0.5 cm were cut from the sheets and drawn at 75°C in an Instron testing machine at a cross head speed of 10 cm/min. Samples with different draw ratios were produced by varying the overall extension applied i.e. the drawing time. The draw ratio obtained was determined from the spacing of ink marks which were applied to the samples before drawing. Further details of the drawing procedure have been given in previous publications^{1,2}.

Hydrostatic extrusion. Billets for hydrostatic extrusion were machined from isotropic rods, prepared by an extrusion moulding technique. In this technique a cylindrical tube is filled from a melt extruder and then allowed to cool over a period of several hours in an oven maintained at 120°C . To prevent the formation of voids in the mouldings it was found beneficial to stand the tubes vertically in the

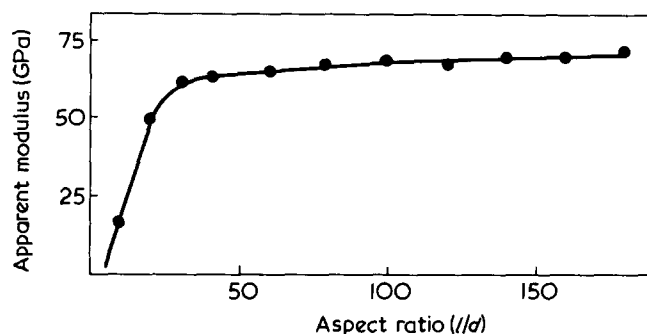


Figure 1 The apparent dynamic modulus measured in 3 point bending as a function of aspect ratio for a sample of Rigidex 50 of deformation ratio 25:1

oven to maintain a temperature gradient of about 10°C up the tube (the top end being hotter) and to apply a small pressure by placing weighted pistons in the top ends of the tubes.

The technique for hydrostatic extrusion of polymers has been described previously^{3,6}. In the present work a conical die of 15° semi-angle was used, the final bore diameter being 2.5 mm. For extrusion we will define the deformation ratio as the cross-sectional area of the billet divided by that of the product. For the samples described here, the product diameter was always fairly close to the bore diameter of the die. All samples were extruded at 100°C.

Characterization of samples

The densities of the samples were determined using a density gradient column and crystallinity values calculated assuming a two phase model with $\rho_c = 1.00$ and $\rho_a = 0.855$ g/cm³.

Wide-angle X-ray diffraction patterns of all samples were recorded on Polaroid film to enable a comparative visual assessment of crystallite orientation to be made. We have also drawn on the more detailed X-ray diffractometry data of the related publication to provide estimates of \bar{D}_{002} , the average crystalline dimension in the *c* direction.

Finally, small-angle X-ray diffraction patterns were recorded for all samples, and the long period, *L*, determined from microdensitometer traces of the peak profiles.

Dynamic mechanical measurements

Dynamic mechanical measurements in the temperature range -196° to 80°C were undertaken on all samples to obtain E^* , the dynamic Young's modulus in the axial direction. All measurements were performed at 3.6 Hz.

The technique for measuring drawn films has already been reported in a previous publication⁴ where data for similar, but not identical samples, have been reported.

For the extruded samples, a three point bend technique was used for two reasons. First, the loads required in flexure are considerably lower than those required for tensile measurements and secondly, problems had been encountered previously in gripping specimens for tensile tests.

Horgan⁷ and Arridge and Folkes⁸ have pointed out that St Venant's principle in its commonly stated form does not apply to highly anisotropic materials. Localized stresses at specimen loading points (end effects) can persist for distances of up to $(E/G)^{1/2}$ times the basic dimension (the diameter in this case) and can lead to appreciable errors in mechanical measurements if allowance is not made for them.

In the three point bend test there is also a deflection due to shear, which is frequently ignored for isotropic materials, but which can be significant when the ratio E/G is large. Fortunately the errors due to both these effects can be reduced to an acceptable level by using a sample of sufficiently large length to diameter ratio.

Neglecting end effects and shear effects, the modulus of a sample in the three point bend test is given by:

$$E = \frac{Wl^3}{48\delta I} \quad (1)$$

where *W* is the load applied at the centre of the specimen; *l* is the distance between supports; δ is the deflection at this point and *I* is the second moment of area of the specimen cross-section about the neutral axis. For a specimen of circular section:

$$I = \frac{\pi d^4}{64} \quad (2)$$

where *d* is the diameter.

In order to minimize errors due to end and shear effects the apparent modulus from equation (1) was measured for a range of aspect ratios for the most highly anisotropic sample and is shown plotted against l/d in Figure 1. Although the error is large at low aspect ratios it can be reduced to an acceptable level (less than 1%) by using an aspect ratio of 160. This geometry was therefore used in all the tests.

For the dynamic measurements a sinusoidal displacement was applied to the central point of the specimen by a scotch yoke mechanism driven at constant speed, the load and displacement also being measured at this point. Details of the electronics used to measure the phase angle between the load and displacement signals are described elsewhere⁹.

Because *d* appears to the fourth power in equation (2), it is necessary to make allowance for the change in specimen dimensions with temperature during the experiment. The thermal expansion data reported by Mead and Porter¹⁰ for capillary-extruded rods were used for this purpose. The maximum correction to the observed modulus (at -196°C) was 13%. A small correction was also made for the changes in *l* due to thermal strain in the apparatus.

It was found that the thermal history of the sample could significantly affect the measured values of $\tan\delta_E$ in the low temperature (γ) relaxation region. Rapid cooling from room temperature to below -50°C gave high $\tan\delta_E$ values which drifted to a steady value over a period of about 1 h. Cooling fairly slowly on the other hand in steps of 10° or 20°C (to facilitate measurements) gave much more stable behaviour, and values of $\tan\delta_E$ were consistent both going down and coming up in temperature. The latter procedure was therefore adopted.

RESULTS

Characterization

Figure 2 shows the densities of the extruded and drawn samples as a function of the deformation ratio. An initial drop in crystallinity is observed, corresponding to the break-up of the isotropic spherulitic morphology. On further deformation the density increases somewhat, but the overall change for this grade of polymer is quite small. The crystal-

linity of the oriented samples deduced from these densities is about 77%.

The wide-angle X-ray diffraction measurements showed that at deformation ratios of 10 and above the crystalline phase is almost perfectly oriented with *c*-axes parallel to the direction of tensile strain. Quantitative measurements of crystallite orientation determined from X-ray diffractometry of the 002 reflections gave values for the orientation averages which were always very close to those for perfect alignment¹¹.

As already mentioned, average crystal dimensions have been determined by X-ray diffractometry in the related investigation⁵. The results show that there is no apparent change in the lateral dimensions, \bar{D}_{200} and \bar{D}_{020} as determined from the profile of the 200 and 020 reflections, respectively. Measurements of the 002 reflection, on the other hand, show that there is a very appreciable increase in \bar{D}_{002} , which rises to a value of about 460 Å at the highest deformation ratios. These results are summarized in Table 1.

At the lower deformation ratios both drawn and extruded samples showed clear small-angle X-ray diffraction (SAXS) patterns of the two point type, though the intensity decreased very considerably with increasing deformation. Values of the long period, *L*, deduced from the SAXS data are also shown in Table 1. For both sets of samples, *L* falls in the early stages of deformation from its isotropic value to a level which then remains fairly constant at about 200 Å. The discontinuous change in *L* is another indication of the break-up of the initial morphological structure and has been

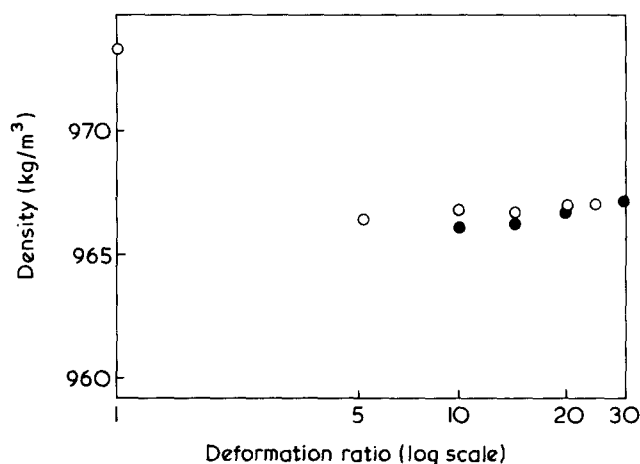


Figure 2 The density of extruded (○) and drawn (●) samples as a function of the deformation ratio

well discussed by previous workers. It is known that *L* depends primarily on the temperature of deformation. Our results are in keeping with this observation since, at a given deformation ratio, we always observe a higher value of *L* in the extruded material than in the drawn material.

Dynamic mechanical behaviour

The variation of the axial storage modulus, E' , and the corresponding loss factor, $\tan\delta_E$, with temperature are shown in Figures 3 and 4 for the extruded samples.

Curves of E' against temperature for specimens of different deformation ratio are similar in shape. All show the two low temperature plateau regions on either side of the γ -relaxation, and the rapid drop in E' with temperature above -50°C due to the onset of the α -relaxation process.

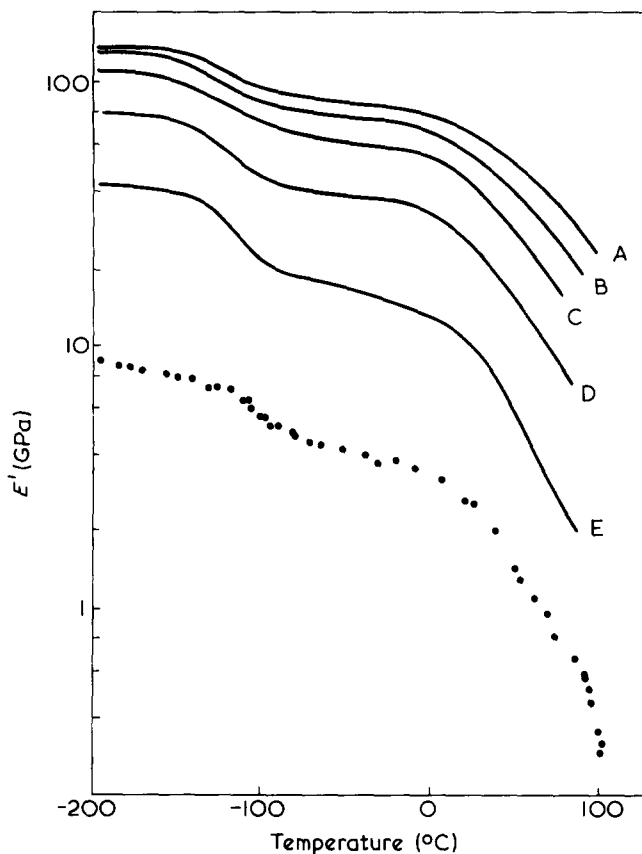


Figure 3 The storage modulus E' at 3.6 Hz as a function of temperature for extruded samples of Rigidex 50. For clarity the data points are shown for the isotropic sample only. Numbers on the solid curves indicate the deformation ratio. A, 25; B, 20; C, 15; D, 10.2; E, 5.18

Table 1 Summary of the X-ray diffraction and dynamic mechanical data for samples of highly oriented linear polyethylene. (E/E_c is calculated assuming $E_c = 255 \text{ GPa}^5$)

Type of sample	Deformation ratio	Long Period, <i>L</i> (Å)	Crystal length, \bar{D}_{002} (Å)	Modulus at -50°C , E (GPa)	ρ	$\frac{E}{E_c}$
Extruded Rigidex 50	5.2	205	228	17	0.053	0.067
	10.2	210	247	38	0.081	0.149
	20	215	349	78	0.238	0.306
Drawn Rigidex 50	9	185	240	32	0.129	0.123
	19	190	410	84	0.367	0.329
	30	198	464	112	0.402	0.439

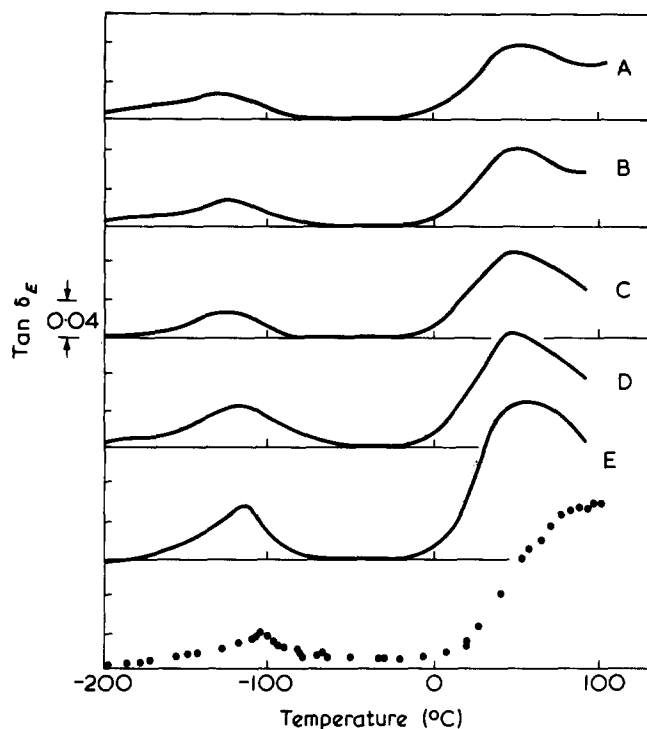


Figure 4 The mechanical loss factor, $\tan \delta E$ corresponding to the data of Fig. 3. Curves have been shifted vertically for clarity. A, 25; B, 20; C, 15; D, 10.2; E, 5.18

This behaviour is qualitatively similar to that reported for many other samples of LPE of widely differing morphology. With the present samples the rate at which E' falls off with temperature in the α region decreases somewhat at higher deformation ratios.

The shape of the α and γ loss peaks in $\tan \delta E$ is fairly similar for all deformation ratios, the changes which occur with increasing deformation ratio being of a secondary nature. The intensity of the γ -relaxation initially increases slightly and then falls off slowly with increasing deformation ratio, the relaxation process becoming spread out over a wider temperature range and moving to a lower temperature. The γ -process is generally acknowledged to contain components due to both the amorphous and crystalline phases, of which the former predominates. The slight initial increase in intensity may therefore be associated with the drop in crystallinity which occurs in the early stages of deformation.

The broadening of the γ -relaxation with increasing deformation ratio probably indicates an increase in the variety and amount of crystalline disorder.

The high temperature α -process also moves to a slightly lower temperature and decreases in intensity, although it shows no sign of disappearing, even in the most highly oriented samples.

The dynamic tensile behaviour of the drawn samples is similar to that of the extruded samples. The main features were reported in a previous publication where a range of samples was prepared by different preparation procedures⁴.

The plateau regions which occur in E' will be referred to as regions 1 and 2. Region 1 refers to the plateau which occurs at -50°C (at the present measurement frequency) and region 2 refers to the plateau below the γ -relaxation. Although the γ -relaxation extends somewhat below the low temperature limit of the apparatus using liquid nitrogen as a coolant, the value of E' at -150°C will be taken

as representative of the region 2 plateau modulus.

Because the temperature and frequency dependence of mechanical behaviour is lowest in the plateau regions, the values of E' in these regions are useful quantities for characterizing the material since they are minimally dependent on the type of measurement technique used. The room temperature modulus, on the other hand, although significant from a practical engineering viewpoint, also reflects shifts in the position and intensity of the α process and can therefore be less easily related to structural parameters.

Values of the storage modulus in plateau regions 1 and 2 and at room temperature are plotted as a function of deformation ratio in Figure 5. It is seen that for a given deformation ratio drawn samples exhibit a slightly higher modulus than extruded samples. This is primarily a reflection of the higher temperature at which the extrusion process was performed.

DISCUSSION

Structural considerations and a morphological model

Considering the likely structural features of these highly deformed LPE samples it is necessary to reconcile two important experimentally observed facts: (a) At high deformation ratios the material retains a periodic density fluctuation as indicated by the SAXS patterns; (b) The average

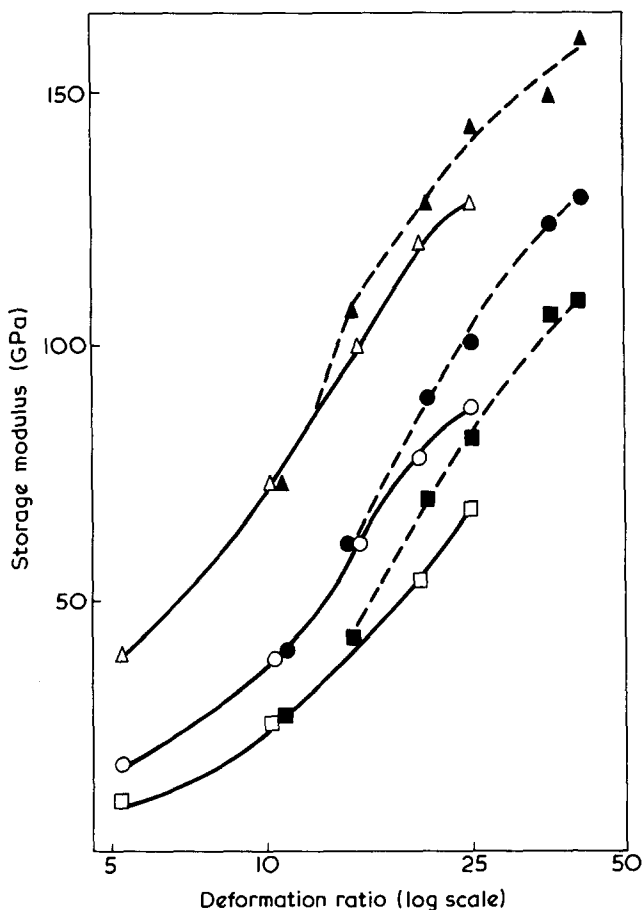


Figure 5 The storage modulus as a function of deformation ratio at room temperature and in the plateau regions 1 and 2. (\square , \circ , \triangle) refer to extruded samples and (\blacksquare , \bullet , \blacktriangle) to drawn samples: \square room temperature data; \circ -50°C data (region 1); \triangle -150°C data (region 2)

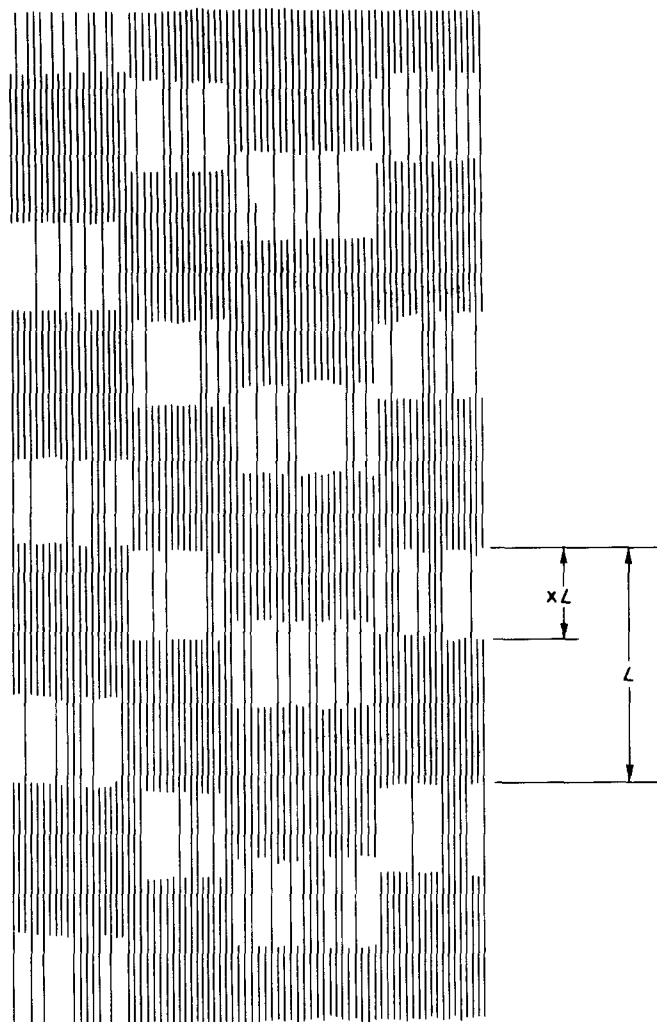


Figure 6 A schematic representation of the structure of the crystalline phase of highly oriented linear polyethylene

value of the c direction crystal thickness, \bar{D}_{002} increases with increasing deformation, and, more importantly, this quantity is consistently greater than the SAXS long period, L .

The structural model which we propose to explain these observations is shown schematically in Figure 6. For convenience the polymer backbone chains are represented by lines, and only the part of the material which is crystalline (from an X-ray diffraction viewpoint) has been shown.

This morphology may be regarded equally well as consisting of fibrillar stacks of crystallites, linked by intercrystalline bridges (as proposed by Fischer *et al.*¹²), or as a continuous crystal containing disordered regions which are periodic in the c direction. In either case, the crystalline phase is essentially continuous in the c direction, the degree of continuity increasing with increasing deformation ratio.

It is likely that the high mechanical stiffness of these materials is due primarily to crystalline continuity rather than to the presence of taut tie molecules. Undoubtedly, such entities exist, along with tight and loose chainfolds and all the other components which make up the amorphous phase in semicrystalline polymers, but at temperatures above that of the primary dispersion of the amorphous phase, it is highly unlikely that they contribute significantly to mechanical behaviour. Quantitative evidence for this will be presented later in our discussion of mechanical behaviour. At temperatures above that of the γ -relaxation,

therefore, the mechanical behaviour probably approximates to that of a continuous crystal containing voids.

The lateral distance over which the structure shown in Figure 6 retains its periodic register is probably of the same order as the quantities \bar{D}_{200} and \bar{D}_{020} described in ref 5, i.e. about 110 Å.

It should be borne in mind that \bar{D}_{002} is in fact an average value, since there is likely to be a distribution of crystal lengths in the c direction. In making an interpretation of the mechanical behaviour in terms of the structure it would be useful to have information about the distribution of crystal lengths and also about the distribution of intercrystalline bridges across the disordered interface. This type of information is not available at present, but an attractive alternative is to proceed on the basis that the intercrystalline material is randomly dispersed.

Consider a chain within the crystalline phase and let p be the probability that this chain will traverse the disordered region to enter an adjacent crystallite. p therefore represents the area fraction of intercrystalline bridge material which traverses the disordered layer. The probability that a particular crystalline sequence will link n blocks is then:

$$f_n = p^{n-1}(1-p) \quad (3)$$

since the sequence must traverse $n-1$ boundaries and fail to traverse one boundary. f_n also represents the number-fraction of crystalline sequences which link n crystallites. The above argument is analogous to the well-known treatment of polymerization by a stepwise condensation reaction¹³.

The weight fraction of chains, F_n , which link n crystallites can be obtained by multiplying f_n by the sequence length and renormalizing. If the thickness of the disordered region (Figure 6) is xL , then the length of a chain linking n crystallites is $(n-x)L$, and F_n is given by:

$$F_n = \frac{(n-x)Lf_n}{\sum_{n=1}^{\infty} (n-x)Lf_n} = \frac{(n-x)p^{n-1}(1-p)^2}{1-x(1-p)} \quad (4)$$

Since the integral breadth of the 002 reflection essentially measures a weight-average chain length (see Appendix I) then:

$$\bar{D}_{002} = \sum_{n=1}^{\infty} F_n(n-x)L \quad (5)$$

We do not know the value of x , but if we ignore the thickness of the disordered region and assume $x \ll 1$ then equations (4) and (5) simplify to:

$$F_n = np^{n-1}(1-p)^2 \quad (6)$$

and

$$\frac{\bar{D}_{002}}{L} = \frac{1+p}{1-p} \quad (7)$$

Equation (7) is the basis of our estimation of p from the X-ray data of ref 5, since rearrangement gives:

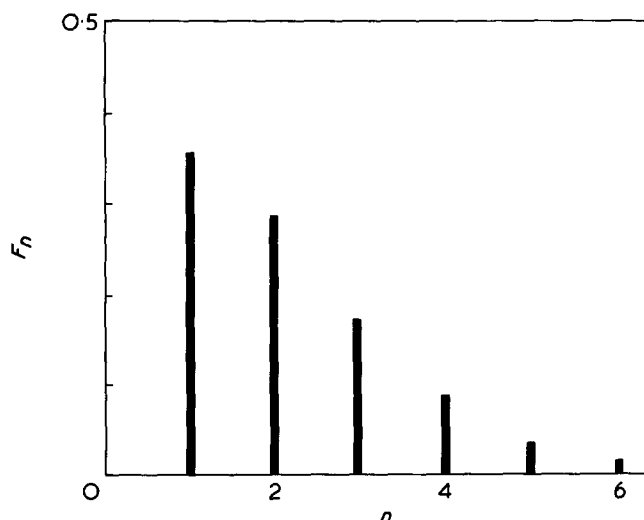


Figure 7 Histogram showing relationship between weight fraction, F_n , of crystalline chains spanning n units, and n , calculated for $p = 0.4$

$$p = \frac{\bar{D}_{002} - L}{\bar{D}_{002} + L} \quad (8)$$

Values of p calculated on this basis* have been included in Table 1, where it can be seen that p increases with deformation ratio from 0.053 in the case of the lowest deformation ratio extruded sample up to 0.402 in the case of the 30:1 drawn sample.

It is seen intuitively that the parameter p is a suitable normalized measure of crystalline continuity, the value of which would vary from zero for a sample with a perfect series arrangement of phases up to unity for the perfect crystal.

Figure 7 shows a distribution of crystalline sequence lengths calculated from equation (6) assuming that $p = 0.4$. It is apparent that less than half of the crystalline phase is in the form of short ($n = 1$) lamellar crystals. Of the rest, there are significant amounts at lengths of up to about $n = 5$ (i.e. about 1000 Å) but no chain-extended material.

Interpretation of mechanical behaviour: general considerations

Present understanding of the relationship between mechanical properties and structure in crystalline polymers is only at the semiquantitative stage. This is due primarily to the high mechanical anisotropy of the crystalline regions, which makes the overall mechanical behaviour extremely sensitive to the shape and disposition of the crystalline phase. This is shown in the present case by the large increase in stiffness which takes place at deformation ratios greater than 10. Above this deformation ratio, the crystalline phase can be regarded as perfectly oriented, and the density changes only by a small amount, so the large change in modulus must be due to a change in the topology

* As an alternative to the simplifying assumption ($x \ll 1$) which led to equation (7) it is possible by observing that the volume fraction crystallinity is $1 - (1 - p)x$, and by using crystallinity values, say from density, to obtain p by solving equations (4) and (5). However the values obtained by this method are fairly similar to those from equation (8) so the simpler method was adopted for brevity.

rather than a change in orientation or concentration of this phase.

It is necessary to mention at this point a previous attempt⁴ to model the mechanical behaviour using the well-known Takayanagi model¹⁴. Using values for the concentration of the amorphous fraction determined from broad line nuclear magnetic resonance (n.m.r.)¹⁵ measurements it was possible to explain the mechanical behaviour of drawn samples of LPE in terms of a series arrangement of phases, the increase in stiffness being attributed to a decrease in concentration of the mobile fraction.

In this model the crystalline phase was not regarded as being continuous. Recent more extensive n.m.r. measurements, however, have shown that a large decrease in mobile fraction is not a general feature of the drawing behaviour of LPE. Moreover, the results of a number of other measurements indicate that an increase in crystalline continuity provides a better explanation for the observed changes in properties.

We have, for instance, undertaken thermal conductivity measurements on hydrostatically extruded materials¹⁶ and have shown that the high axial thermal conductivity which develops on tensile deformation is consistent with an increase in crystalline continuity, i.e. an increase in the fraction of intercrystalline bridge material.

More recently, X-ray diffraction measurements of crystal strain in drawn materials under load, a preliminary account of which has already been published¹⁷, and which are described in detail in the accompanying paper⁵ provide definitive evidence that the series type of model is incorrect for LPE, and indeed the room temperature crystal strain results would be more consistent with a 'constant strain' or parallel model.

As mentioned already, the average crystal thickness can increase to a value which is several times the long period, but nevertheless the material does not contain any significant amount of extended-chain material, so the material behaves as a network of highly anisotropic crystals of various lengths. These considerations lead us to consider the relevance of a model based on an aligned fibre composite material. More specifically, we shall seek to show how the intercrystalline bridge content, p , estimated on the basis of the model described, can be used to provide a direct link between mechanical properties and structure.

Mechanical behaviour of the proposed morphological model in terms of composite theory

Halpin and Kardos¹⁸ suggested that partly crystalline polymers are similar to composite materials where a fibrous filler is dispersed in a matrix of lower stiffness. The increase in Young's modulus on tensile deformation can then be attributed to an increase in the aspect ratio of the crystalline regions which act as the filler. Halpin and Kardos proposed the use of the Halpin-Tsai equation¹⁹, which contains a parameter related to the aspect ratio of the reinforcing phase.

A fundamental problem when attempting to apply composite theory to a polymeric material is one of deciding what constitutes the 'fibre' and 'matrix' in the structural analogue. A simplistic approach would be to equate the crystalline and amorphous phases with the fibre and matrix. This approach has been used with a degree of success for low crystallinity polymers where the amorphous phase is clearly the continuous phase, but the morphological evidence in the case of ultra-oriented LPE tends to indicate

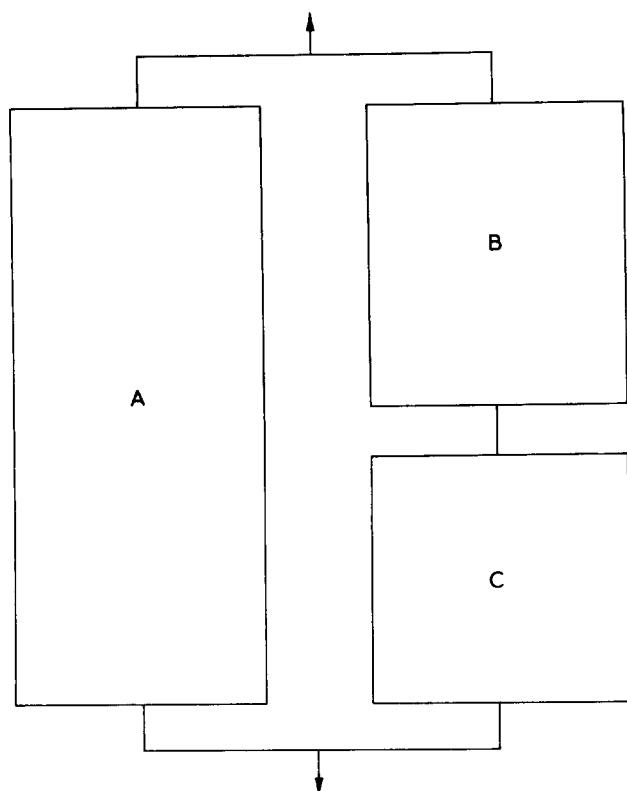


Figure 8 The assumed mechanical connectivity of the fibre phase (A) lamellar phase (B) and amorphous phase (C) of highly oriented LPE

that the crystalline phase is continuous in this material, so the problem warrants further consideration.

For the present case, where the material is known to contain highly oriented crystalline sequences of various lengths, it seems more appropriate to draw an analogy with an aligned fibre composite. Cox²⁰, Dow²¹ and Rosen²² have all proposed theories for the stresses in discontinuous fibres incorporated in a relatively soft matrix. There are some inconsistencies between the different approaches, but all three workers consider that in the vicinity of each fibre end the fibre tensile stress falls to zero, load being transferred by shear to the matrix. The original version of 'shear lag' theory, as it has become known, will be mentioned here by way of illustration.

Using Cox's theory, the modulus of an aligned short fibre composite is given by:

$$E = E_f V_f \left[1 - \frac{\tanh B}{B} \right] + E_m V_m \quad (9)$$

where E_f and E_m are the Young's moduli of fibre and matrix components, respectively, whose volume fractions are V_f and V_m . The quantity B is given by:

$$B = \left[\frac{2l_f}{d_f} \right] \left[\frac{G_m}{E_f} \right]^{1/2} \left\{ \frac{1}{\ln[2\pi(3V_f)^{1/2}]} \right\}^{1/2} \quad (10)$$

where l_f and d_f are the fibre length and diameter and G_m is the shear modulus of the matrix phase.

This expression shows that the composite behaviour is determined by three factors: (i) the aspect ratio of the reinforcing phase; (ii) the ratio G_m/E_f ; (iii) the fibre volume fraction.

For convenience we will define a 'shear lag' factor, ϕ , where:

$$\phi = 1 - \frac{\tanh B}{B} \quad (11)$$

so the composite modulus is given by:

$$E = E_f V_f \phi + E_m V_m \quad (12)$$

In the following discussion the mechanical behaviour will be described in terms of the shear lag factor. We are not relying specifically on the validity of Cox's model, since the other models also give expressions like equation (12) for the overall modulus.

Equation (12) is seen to be similar to the familiar 'uniform strain' expression, but with the fibre term modified by the factor ϕ to allow for the finite aspect ratio of this phase. ϕ can be regarded, therefore, as an efficiency factor for the reinforcing phase. Alternatively we may invoke the concept of 'ineffective length', observing that a fraction $(1 - \phi)$ of the reinforcing phase is ineffective in transmitting stress, there being an 'ineffective length' of $(1 - \phi)l_f/2$ at the end of each fibre.

It is to be expected that only those crystalline chains which cross interlamellar boundaries will contribute significantly to mechanical stiffness, so the 'matrix' may be regarded as consisting of a mixture of chain-folded and disordered material. This arrangement is shown schematically in Figure 8, where the concentration, V_f , of the fibre phase is identified with that of the crystalline sequences where $n > 1$. The main difficulty with this type of approach, advocated independently by Barham and Arridge²³ and by Gibson⁶ is that the increase in stiffness which occurs as a result of tensile deformation can be interpreted as being due either to an increase in l_f/d_f or to an increase in V_f . Another problem with models based directly on theory for short fibres is that a single fibre aspect ratio is assumed, when in fact a distribution of aspect ratios is more likely as already mentioned. It is also difficult to envisage how 'fibres' consisting of perfectly crystalline material could increase in aspect ratio as a result of tensile deformation.

In the present model, increases in length of and amount of 'fibre' phase are interrelated so composite theory conclusions can be made which are compatible with the X-ray data already discussed.

It should be emphasized that we do not envisage the reinforcing fibre phase as discrete identifiable entities which retain their identity throughout the drawing process. At each stage of the deformation there is a degree of crystal continuity which can be represented by an apparent fibrillar content. Although we do not discuss here the mechanisms leading to the formation of the proposed morphology, we consider that they are probably similar to those originally outlined by Peterlin²⁴.

If we treat each chain which links at least two lamellae as a reinforcing fibre then the volume of the fibre phase V_f and the lamellar ($n = 1$) phase, V_l are given by:

$$V_f = \chi \sum_{n=2}^{\infty} F_n = \chi p(2 - p) \quad (13)$$

$$V_l = \chi F_1 = \chi(1 - p)^2 \quad (14)$$

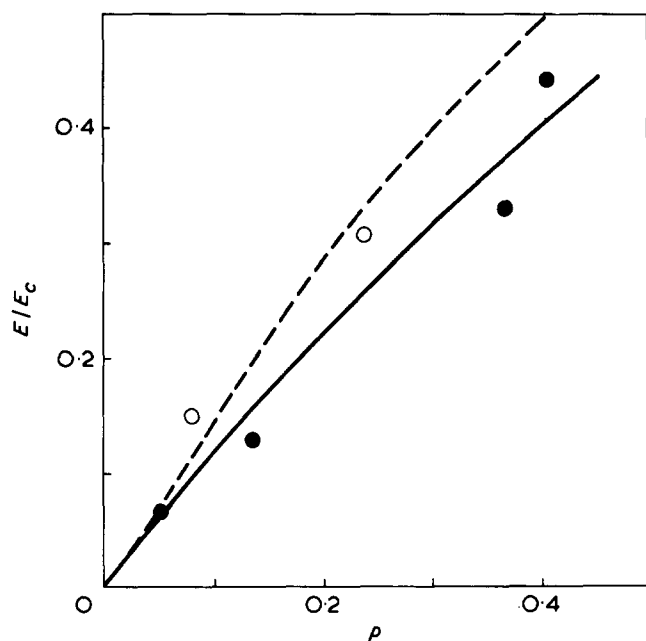


Figure 9 A comparison between the experimental data at -50°C and the predictions of equation (20). \circ extruded samples, \bullet drawn samples. Broken line $\chi\phi' = 0.77$, solid line $\chi\phi' = 0.6$

and equation (12), modified to take account of the distribution of fibre lengths, becomes:

$$E = \chi E_c \sum_{n=2}^{\infty} F_n \phi_n + \{(1 - \chi) + \chi F_1\} E_m \quad (15)$$

where ϕ_n is the shear lag factor for chains of length nL , E_c is the tensile modulus of the perfect crystal and χ is the volume crystallinity.

It is convenient to define an average shear lag factor ϕ' such that:

$$E = \chi(1 - F_1)E_c\phi' + E_m V_m \quad (16)$$

$$\text{hence } \phi' = \frac{1}{1 - F_1} \sum_{n=2}^{\infty} F_n \phi_n = \frac{1}{p(2 - p)} \sum_{n=2}^{\infty} F_n \phi_n \quad (17)$$

Also, considering Figure 8, it is reasonable to assume that the matrix extensional modulus, E_m , may be obtained by a series addition of the two components. Hence:

$$\frac{\chi(1 - p)^2 + (1 - \chi)}{E_m} = \frac{\chi(1 - p)^2}{E_c} + \frac{(1 - \chi)}{E_a} \quad (18)$$

Finally we obtain an expression for the sample modulus, combining equations 13–18 to yield:

$$\frac{E}{E_c} = \chi p(2 - p)\phi' + \frac{\{(1 - \chi) + \chi(1 - p)^2\} E_a/E_c}{(1 - \chi) + \chi(1 - p)^2 E_a/E_c} \quad (19)$$

An important aspect of equation (19) is that as the ratio E_a/E_c tends to a low value, the second term, representing the tensile contribution of the matrix to the overall stiff-

ness becomes small compared with the first. It will later be argued that at temperatures above that of the γ -relaxation this is the case, and behaviour is dominated solely by the crystalline 'fibre' term, equation (19) reducing to:

$$\frac{E}{E_c} = \chi p(2 - p)\phi' \quad (20)$$

Comparison of experimental and theoretical moduli

In comparing the theoretical and experimental moduli it is tempting to analyse the room temperature data. As mentioned previously, however, this is undesirable as the material is viscoelastic at room temperature and low frequencies (say <100 Hz) and the room temperature modulus is therefore strongly affected by the shifts in the position and intensity of the α process which occur on deformation. We have concentrated instead on the behaviour in the plateau region 1 around -50°C , where the material is essentially elastic at all frequencies of interest and where the modulus shows only a weak dependence on temperature and frequency.

The experimental moduli at -50°C , normalized to the form E/E_c (assuming $E_c = 255$ GPa), have been added to Table 1, where it can be seen that, like the parameter p , they increase systematically with increasing deformation ratio for the two sets of samples. Figure 9 shows that there is a good correlation between E/E_c and p for the two sets of samples.

The comparison between the experimental moduli and the values predicted by equations (19) or (20) is complicated somewhat by the problem of deciding upon realistic crystallinity values for the samples. On the one hand, density measurements (assuming the customary two phase model) indicate a figure of ~ 0.77 whilst the crystal strain measurements⁵ suggest a figure as low as 0.60 for drawn samples of intermediate draw ratio, rising to 0.70 for the most highly drawn sample.

To some extent this problem is artificial in that if we assume the lower value for crystallinity then the 'amorphous' phase has to have a higher density than that usually assumed and it will probably be relatively highly oriented. Bearing this in mind, it is now necessary to consider the validity of the approximation $E_a \ll E_c$ made in the last section and which led to equation (20).

If the matrix contribution to the tensile modulus is insignificant at -50°C , then extrapolation of the data in Figure 9 to $p = 0$, corresponding to a 'parallel lamella' structure with no crystalline continuity, should give a near-zero value of E/E_c . Examining the actual points, this condition does appear to be satisfied. Taking account of experimental scatter, the data could quite reasonably be considered to pass through the origin. A maximum reasonable value for the intercept would be about 0.05, so we may safely say that $E_m < 0.05 E_c$. Since, at very low values of p the matrix modulus approaches a value of $E_a/(1 - \chi)$ we may estimate that $E_a < 0.02 E_c$.

Our approximation seems, therefore, to be adequately justified and our previous claim that the disordered regions function as voids at -50°C and above can be upheld.

We now return with confidence to equation (20) which predicts that the stiffness is directly proportional to the product $\chi\phi'$. The fit obtainable from equation (20) is illustrated by the two lines in Figure 9 which were calculated for $\chi\phi' = 0.77$ (broken line) and $\chi\phi' = 0.60$ (solid line), the latter being the better fit to the data. We can therefore conclude that the behaviour at -50°C lies somewhere between

the following extremes: (1) crystallinity is 0.6 and 'shear lag' effects at -50°C are insignificant (i.e. $\phi' = 1$); (2) crystallinity is 0.77, but shear lag reduces the effectiveness of the reinforcing phase ($\phi' = 0.6/0.77 = 0.78$).

Shear lag effects, therefore, are only of secondary importance in determining the modulus at -50°C , and the modulus increase with increasing draw ratio can be attributed mainly to the large increase in the term $\chi p(2-p)$, which in turn is primarily due to an increase in p . We have arrived at a fairly simple picture of the situation in which modulus is primarily determined by the volume, V_f , of the fibre phase. The matrix contributes an insignificant amount to the tensile properties, but it has sufficient resistance to shear to transfer the stress efficiently from fibre to fibre. The discussion can profitably be carried forward further to consider the respective roles of the lamellar crystals ($n = 1$) and amorphous material.

Calculations, based on measurements of shear modulus as well as tensile modulus, show that the shear modulus of the matrix at -50°C is primarily determined by the lamellar material. These results, which will be reported in detail elsewhere²⁵, indicate that the stress transfer in shear takes place predominantly via the crystalline component.

Interpretation of γ and α relaxation processes

A useful aspect of the composite theory approach is that it offers some fairly straightforward interpretations of the α and γ relaxations in these materials. The modulus change in the low temperature γ region, can be primarily attributed to a substantial change in the tensile modulus of the amorphous phase. This comes from the following considerations.

Variations in E_c over the temperature range in question are likely to be small, as has been confirmed by crystal strain measurements on an annealed sample⁵. We have already shown that at -50°C the lowest reasonable value of ϕ' is 0.78, so the 'fibre' term in equation (19) is capable of a 28% increase at the most when going from -50° to -150°C . It is likely, therefore, that the greater part of the stiffness increase in the γ region is due to the 'matrix' term in equation (19) becoming significant. We can determine the approximate value of E_a at -150°C from the sample modulus change between -50° and -150°C . If we neglect the effect of changes in ϕ' and assume that $\chi = 0.6$ we find that E_a/E_c at -150°C changes from ~ 0.1 for the lowest deformation ratio up to ~ 0.2 for the highest deformation ratio. Changes in ϕ' have a greater effect at higher deformation ratios where the fibre term is larger, and if allowance is made for such changes, the estimate of E_a/E_c at higher deformation ratios is reduced somewhat. Nevertheless, it does appear that the value of E_a increases with increasing deformation, which is in keeping with the increase in amorphous orientation observed in broad line n.m.r. measurements¹¹. It is noted in passing that the maximum estimate of E_a , 51 GPa, is very high for an oriented polymer phase in the glassy state.

The second order effect, the increase in ϕ' , can be expected to have two components due to the change in shear moduli of the amorphous and lamellar ($n = 1$) crystalline components, both of which will affect G_m . It is necessary to make some allowance especially for the latter effect: since we have discounted variations in E_c , the crystalline component of the γ relaxation can only operate through changes in the matrix shear modulus. This effect probably accounts for the small residual slope of the modulus-temperature plot below the main γ relaxation as well as the broad background observed in $\tan\delta_E$.

Turning now to the α -process, the approximation that $E_a \ll E_c$ can be made with confidence in this temperature region. The fall in sample modulus can only be due, in terms of the model to a fall in the value of ϕ' which in turn indicates a fall in the matrix shear modulus. The calculation of ϕ' from first principles is, however, quite difficult in view of the complicated sample morphology. Within the confines of the present model one may assume a constant ineffective length mL , say, irrespective of the fibre length. We may then calculate ϕ_n from:

$$\phi_n = \frac{n-m}{n} \quad (n > 2m) \quad (21)$$

For short fibres in which the maximum stress of a long fibre is never reached, a simple triangular stress profile may be assumed with a stress decay rate equal to the maximum stress attained in a long fibre divided by the ineffective length. This yields:

$$\phi_n = \frac{n}{4m} \quad (n < 2m) \quad (22)$$

The details of this latter calculation are not important at high values of p since the modulus is mainly dependent upon the concentration of long fibres.

Calculations of ϕ' on this basis show that the room temperature data for the highest deformation ratio samples may be fitted with a value of m of the order of one, thus indicating an ineffective length of about 200 Å in these samples. Most of the stress transfer between fibres therefore occurs through the crystal lamellae in which one fibre ends and another begins. The decreasing value of ϕ' with increasing temperature is consistent, therefore, with the interpretation of the α process as a crystal shear process. It is only at the highest temperatures where m is much greater than 1 that we need to consider the problem of determining the shear modulus of the matrix phase.

In the α -region, the composite model has a distinct advantage over the previous models involving only tensile moduli because it shows how the overall tensile behaviour is a reflection of the *shear* behaviour of the matrix. This may go some way to explaining the qualitative similarity of the α peaks in $\tan\delta_E$ in LPE samples having widely differing morphologies.

Application to crystal strain measurements

In the accompanying publication⁵ the apparent crystal modulus, E_c^{app} , has been measured by dividing the sample stress by the crystalline strain measured by X-ray techniques. It is of interest to show that E_c^{app} can be calculated on the basis of the model described here. To do this, we note that the shear lag factor represents the ratio of the mean strain in the fibre phase, $\bar{\epsilon}_f$, to the applied strain, ϵ , so we may write:

$$\bar{\epsilon}_f = \phi' \epsilon \quad (23)$$

The mean strain in the lamellar phase, $\bar{\epsilon}_l$ is calculated by noting that the average strain in the series-connected lamellar and amorphous phases is equal to the applied strain, ϵ . A little algebra soon yields:

$$\bar{\epsilon}_l = \frac{\epsilon \{(1-\chi) + \chi(1-p)^2\} E_a/E_c}{(1-\chi) + \chi(1-p)^2 E_a/E_c} \quad (24)$$

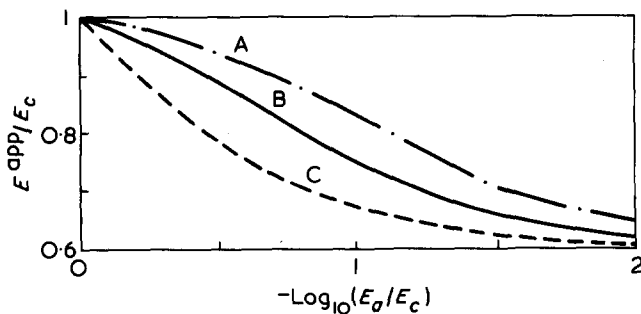


Figure 10 The apparent crystal modulus as a function of E_a/E_c as predicted by equation (24) for different values of p , assuming $\phi' = 1$: A, $p = 0.1$; B, $p = 0.2$; C, $p = 0.5$

The mean crystal strain, $\bar{\epsilon}_c$, is therefore given by:

$$\bar{\epsilon}_c = V_f \bar{\epsilon}_f + V_l \bar{\epsilon}_l \quad (25)$$

which, with the appropriate substitutions, may be written:

$$\frac{\bar{\epsilon}_c}{\epsilon} = p(2-p)\phi' + \frac{(1-p)^2\{(1-\chi) + \chi(1-p)^2\}E_a/E_c}{(1-\chi) + \chi(1-p)^2E_a/E_c} \quad (26)$$

But $E_c^{\text{app}} = \sigma/\bar{\epsilon}_c$ where σ is the sample stress which may be written in terms of the sample modulus and strain. Hence:

$$E_c^{\text{app}} = \frac{\sigma}{\bar{\epsilon}_c} = E \frac{\epsilon}{\bar{\epsilon}_c}$$

$$\text{and } \frac{E_c^{\text{app}}}{E_c} = \frac{E}{E_c} \frac{\epsilon}{\bar{\epsilon}_c}$$

Combining equations (19) and (26) we obtain:

$$\frac{E_c^{\text{app}}}{E_c} = \frac{\chi p(2-p)\phi' + \frac{\{(1-\chi) + \chi(1-p)^2\}E_a/E_c}{(1-\chi) + \chi(1-p)^2E_a/E_c}}{p(2-p)\phi' + \frac{(1-p)^2\{(1-\chi) + \chi(1-p)^2\}E_a/E_c}{(1-\chi) + \chi(1-p)^2E_a/E_c}} \quad (27)$$

We note that as E_a/E_c tends to zero, E_c^{app}/E_c tends to χ , whereas as E_a/E_c tends to 1, then E_c^{app}/E_c also tends to 1. The detailed behaviour between these limits depends upon p and ϕ' as shown in Figure 10, where a crystallinity of 0.6 is assumed in keeping with the general trend of the results of ref 5. For simplicity a value of ϕ' of 1 is assumed which, as discussed, is approximately true for data below -50°C . Figure 10 compares well with the crystal modulus measurements⁵ as a function of temperature for samples of different deformation ratio if we associate increasing E_a/E_c with decreasing temperature and increasing p with increasing deformation ratio. We note that the main features of the crystal strain measurements can be interpreted without involving considerations of shear lag.

CONCLUSIONS

A correlation between the tensile modulus and the average longitudinal crystal thickness has been shown to exist in

samples of ultra-oriented polyethylene. Structural studies suggest that such samples consist of lamellar stacks of crystallites linked by intercrystalline bridges, the concentration of which has been estimated from X-ray diffraction data reported in the related publication⁵. A quantitative model has been proposed which treats the portions of the sample which are linked by intercrystalline bridges as the fibre phase in a fibre reinforced composite material. The major feature of this model is that the modulus at -50°C is determined primarily by the total amount of fibre phase which is a strong function of deformation ratio.

In addition, the model incorporates 'shear lag' effects which are shown to be significant at room temperature, and lead to a satisfactory modelling of the α process as a crystal shear process. The γ process is seen primarily as a change in the tensile modulus of the amorphous phase, with secondary shear lag effects.

ACKNOWLEDGEMENT

One of us (A. G. G.) would like to acknowledge the support of the Science Research Council, in the form of a Postdoctoral Fellowship.

APPENDIX I

Integral breadth of the 002 reflection

If we consider a single chain of r repeat units we may compare its behaviour with a finite diffraction grating with r slits. The intensity of a diffraction maximum is proportional to r^2 and the width is proportional to r^{-1} hence the area is proportional to r .

The integral breadth, β , is defined as the peak area divided by the height and is therefore proportional to r^{-1} .

If we have an assembly of chains of different length, with N_r chains containing r repeat units, then the resultant diffraction maximum profile will depend upon whether the chains diffract coherently or incoherently. Say that, in general, m_r of the N_r chains form a coherently scattering group, then the intensity of the diffraction maximum for these chains, I_r is given by:

$$I_r \propto \frac{N_r}{m_r} (m_r r)^2 \quad (A1)$$

This is because the maximum scattered intensity from a single group of coherent scatterers is proportional to $(m_r r)^2$ and we have N_r/m_r such groups. The integrated area is, however, independent of m_r being merely proportional to $N_r r$, i.e. the total number of scatterers.

We may readily generalize to an assembly of chains of different lengths if we assume that chains of different length scatter incoherently. We then merely have to add the scattered intensities to obtain the maximum intensity. The total integrated area is always proportional to the total number of scatterers. Hence,

$$\beta^{-1} \propto \frac{\sum_{r=1}^{\infty} (N_r/m_r)(m_r r)^2}{\sum_{r=1}^{\infty} N_r r} \quad (A2)$$

that is:

$$\beta^{-1} \propto \frac{\sum_{r=1}^{\infty} N_r m_r r^2}{\sum_{r=1}^{\infty} N_r r} \quad (\text{A3})$$

Basically, m_r describes the lateral width of the cluster of chains and its dependence on r describes the shape of the crystals, e.g. for cubes m_r would be proportional to r^2 . In an essentially fibrillar texture it is reasonable to assume that m_r is independent of r . We may therefore remove it from the sum and obtain:

$$\beta^{-1} \propto \frac{\sum_{r=1}^{\infty} N_r r^2}{\sum_{r=1}^{\infty} N_r r} \quad (\text{A4})$$

In this instance we are interested in a model in which only certain values of r are allowed, i.e. those which correspond to chain lengths which are integral multiples of L , the low-angle repeat distance. We may therefore change from a sum over r to a sum over n where nL is the length of a chain to which the index n refers. If we also use the number fractions f_n of chains, rather than the total number, we obtain:

$$\beta^{-1} \propto \frac{\sum_{n=1}^{\infty} f_n n^2}{\sum_{n=1}^{\infty} f_n n} \quad (\text{A5})$$

Noting that the weight fraction F_n is essentially proportional to $n f_n$ and that the length of a chain ln is given by nL , we may write:

$$\beta^{-1} \propto \frac{\sum_{n=1}^{\infty} F_n l_n}{\sum_{n=1}^{\infty} F_n} \quad (\text{A6})$$

The inverse integral breadth therefore essentially measures a 'weight-average' chain length rather than a number-average if the assumptions made in this Appendix hold. These assumptions are strictly valid for a randomly placed assembly of parallel rod-like crystals of constant area which is similar to the proposed structure of the highly oriented polymers.

REFERENCES

- 1 Capaccio, G. and Ward, I. M. *Nature (Phys. Sci.)* 1973, 243, 143; *Polymer* 1974, 15, 233
- 2 Capaccio, G., Crompton, T. A. and Ward, I. M. *J. Polym. Sci. (Polym. Phys. Edn)* 1976, 14, 1641
- 3 Gibson, A. G., Ward, I. M., Cole, B. N. and Parsons, B. J. *Mater. Sci.* 1974, 9, 1193
- 4 Smith, J. B., Davies, G. R., Capaccio, G. and Ward, I. M. *J. Polym. Sci. (Polym. Phys. Edn)* 1975, 13, 2331
- 5 Clements, J., Jakeways, R. and Ward, I. M. *Polymer* 1978, 19, 639
- 6 Gibson, A. G. *PhD Thesis* Leeds University (1977)
- 7 Horgan, C. O. *J. Elasticity*, 1972, 2, 4, 335
- 8 Arridge, R. G. C. and Folkes, M. J. *Polymer* 1976, 17, 6, 495
- 9 Rushworth, A. *PhD Thesis* Leeds University (1977)
- 10 Mead, W. T. and Porter, R. S. *J. Appl. Phys.* 1976, 47, 10
- 11 Smith, J. B., Manuel, A. J. and Ward, I. M. *Polymer* 1975, 16, 57
- 12 Fischer, E. W., Goddar, H. and Peiszcsek, W. *J. Polym. Sci. (C)* 1971, 32, 149
- 13 Billmeyer, F. W. 'Textbook of Polymer Science', 2nd Edn., Wiley-Interscience, New York 1971, p 267
- 14 Takayanagi, M., Imada, K. and Kajiyama, T. *J. Polym. Sci. (C)* 1966, 15, 263
- 15 Cochran, M. A. unpublished work
- 16 Gibson, A. G., Greig, D., Sahota, M., Ward, I. M. and Choy, C. L. *J. Polym. Sci. (Polym. Lett. Edn)* 1977, 15, 183
- 17 Britton, R. N., Jakeways, R. and Ward, I. M. *J. Mater. Sci.* 1976, 11, 2057
- 18 Halpin, J. C. and Kardos, J. L. *J. Appl. Phys.* 1972, 43, 2235
- 19 Halpin, J. C. and Tsai, S. W. 'Environment Factors in Composite Materials Design', AFML TR 67-423
- 20 Cox, H. L. *Br. J. Appl. Phys.* 1952, 3, 72
- 21 Dow, N. F. GEC Space Science Lab., GEC Missile and Space Divn, Report No. R635061
- 22 Rosen, B. W. 'Fibre Composite Materials', ASM Publications, 1965
- 23 Barham, P. J. and Arridge, R. G. C. *J. Polymer Sci. (Polym. Phys. Edn)* in press
- 24 Peterlin, A. *J. Mater. Sci.* 1971, 6, 490
- 25 Gibson, A. G., Abdul-Jawad, S. M. S., Davies, G. R. and Ward, I. M. to be published